

1  
2  
3  
4  
5  
6  
7  
8  
9  
10  
11  
12  
13  
14  
15  
16  
17  
18  
19  
20  
21  
22  
23  
24

**A Proposed Method for Estimating Interception from Near-Surface Soil  
Moisture Response**

Subodh Acharya<sup>1</sup>, Daniel McLaughlin<sup>2</sup>, David Kaplan<sup>3,\*</sup>, and Matthew J. Cohen<sup>1</sup>

1 – School of Forest Resources and Conservation, University of Florida, Gainesville FL  
2 – Department of Forest Resources and Conservation, Virginia Tech, Blacksburg, VA  
3 – Environmental Engineering Sciences Department, University of Florida, Gainesville FL  
\* – Corresponding Author

## Abstract

Interception is the storage and subsequent evaporation of rainfall by above-ground structures, including canopy and groundcover vegetation and surface litter. Accurately quantifying interception is critical for understanding how ecosystems partition incoming precipitation, but it is difficult and costly to measure, leading most studies to rely on modeled interception estimates. Moreover, forest interception estimates typically focus only on canopy storage, despite the potential for substantial interception by groundcover vegetation and surface litter. In this study, we developed an approach to quantify “total” interception (i.e., including forest canopy, understory, and surface litter layers) using measurements of shallow soil moisture dynamics during rainfall events. Across 34 pine and mixed forest stands in Florida (USA), we used soil moisture and precipitation ( $P$ ) data to estimate interception storage capacity ( $\beta_s$ ), a parameter required to estimate total annual interception ( $I_a$ ) relative to  $P$ . Estimated values for  $\beta_s$  (mean  $\beta_s = 0.30$  cm;  $0.01 \leq \beta_s \leq 0.62$  cm) and  $I_a/P$  (mean  $I_a/P = 0.14$ ;  $0.06 \leq I_a/P \leq 0.21$ ) were broadly consistent with reported literature values for these ecosystems and were significantly predicted by forest structural attributes (leaf area index and percent groundcover), as well as other site variables (e.g., water table depth). The best-fit model was dominated by LAI and explained nearly 80% of observed  $\beta_s$  variation. These results suggest that whole-forest interception can be estimated using near-surface soil moisture time series, though additional direct comparisons would further support this assertion. Additionally, variability in interception across a single forest type underscores the need for expanded empirical measurement. Potential cost savings and logistical advantages of this proposed method relative to conventional, labor-intensive interception measurements may improve empirical estimation of this critical water budget element.

48

## Introduction

49           Rainfall interception ( $I$ ) is the fraction of incident rainfall stored by above-ground  
50 ecosystem structures (i.e., vegetation and litter layers) and subsequently returned to the  
51 atmosphere via evaporation ( $E$ ), never reaching the soil surface and thus never directly  
52 supporting transpiration ( $T$ ) [Savenije, 2004]. Interception depends on climate and vegetation  
53 characteristics and can be as high as 50% of gross rainfall [Gerrits *et al.*, 2007; 2010; Calder,  
54 1990]. Despite being critical for accurate water budget enumeration [David *et al.*, 2006],  
55 interception is often disregarded or lumped with evapotranspiration ( $ET$ ) in hydrological models  
56 [Savenije, 2004]. Recent work suggests interception uncertainty constrains efforts to partition  $ET$   
57 into  $T$  and  $E$ , impairing representation of water use and yield in terrestrial ecosystems [Wei *et al.*,  
58 2017].

59           When interception is explicitly considered, it is typically empirically estimated or  
60 modeled solely for the tree canopy. For example, direct measurements are often obtained from  
61 differences between total rainfall and water that passes through the canopy to elevated above-  
62 ground collectors (throughfall) plus water that runs down tree trunks (stemflow) during natural  
63 [e.g., Bryant *et al.*, 2005, Ghimire *et al.*, 2012, 2016] or simulated [e.g., Guevara-Escobar *et al.*,  
64 2007; Putuhena and Cordery, 1996] rainfall events. This method yields the rainfall fraction held  
65 by and subsequently evaporated from the canopy but ignores interception by understory  
66 vegetation and litter. Alternatively, numerous empirical [e.g., Merriam, 1960], process-based  
67 [e.g., Rutter *et al.*, 1971, 1975; Gash, 1979, 1995, Liu, 1998], and stochastic [Calder, 1986]  
68 models are available for estimating interception. As with direct measurements, most model  
69 applications consider only canopy storage despite groundcover (both understory vegetation and  
70 litter layers) interception that can exceed canopy values in some settings [Gerrits and Savenije,

71 2011; *Putuhena and Cordery*, 1996]. As such, it seems likely that conventional measures and  
72 typical model applications underestimate actual (i.e., “total”) interception.

73         New field approaches are needed to improve quantification of total interception and  
74 refine the calibration and application of available models. A detailed review of available  
75 interception models [*Muzylo et al.*, 2009] stresses the need for direct interception measurements  
76 across forest types and hydroclimatic regions, but meeting this need will require substantial  
77 methodological advances. Throughfall measurements yield direct and site-specific interception  
78 estimates [e.g., *Ghimire et al.*, 2017; *Bryant et al.*, 2005], but they are difficult and costly to  
79 implement even at the stand scale because of high spatial and temporal variability in vegetation  
80 structure [*Zimmerman et al.*, 2010; *Zimmerman and Zimmerman*, 2014]. Moreover,  
81 comprehensive measurements also require enumeration of spatially heterogeneous stemflow, as  
82 well as interception storage by the understory and litter layers, greatly exacerbating sampling  
83 complexity and cost [*Lundberg et al.*, 1997]. Empirical techniques that estimate total interception,  
84 integrate across local spatial and temporal variation, and minimize field installation complexity  
85 are clearly desirable.

86         Here we present a novel approach for estimating total (i.e., canopy, understory and litter)  
87 interception using continuously logged, near-surface soil moisture. Prior to runoff generation,  
88 infiltration is equivalent to rainfall minus total interception, and the response of near-surface soil  
89 moisture during and directly following rain events can be used to inform interception parameters  
90 and thus interception. Since soil moisture is relatively easy and economical to measure  
91 continuously for extended periods, successful inference of interception from soil moisture time  
92 series may greatly expand the temporal and spatial domains of empirical interception  
93 measurements. As a proof-of-concept, we tested this simple interception estimation method in 34

94 forest plots spanning a wide range of conditions (e.g., tree density, composition, groundcover,  
95 understory management, age, and hydrogeologic setting) across Florida (USA).

96

97

## Methods

### 98 Estimating Interception Storage Capacity from Soil Moisture Data

99 During every rainfall event, a portion of the total precipitation ( $P$ ) is temporarily stored in  
100 the forest canopy and groundcover (hereafter referring to both live understory vegetation and  
101 forest floor litter). We assume that infiltration (and thus any increase in soil moisture) begins  
102 only after total interception storage, defined as the sum of canopy and groundcover storage, is  
103 full. We further assume this stored water subsequently evaporates to meet atmospheric demand.  
104 Calculating dynamic interception storage requires first determining the total storage capacity  
105 ( $\beta_s$ ), which is comprised of the storage capacities for the forest canopy ( $\beta_c$ ) and groundcover ( $\beta_g$ )  
106 (Fig. 1a).

107 To estimate  $\beta_s$ , we consider a population of individual rainfall events of varying depth  
108 over a forest for which high frequency (i.e., 4 hr<sup>-1</sup>) soil-moisture measurements are available  
109 from near the soil surface. To ensure that canopy and groundcover layers are dry, and thus  
110 interception storage is zero prior to rainfall onset (i.e., antecedent interception storage capacity =  
111  $\beta_s$ ), we further filter the rainfall data to only include the events that are separated by at least 72  
112 hours. Volumetric soil water content ( $\theta$ ) at the sensor changes only after rainfall fills  $\beta_s$ ,  
113 evaporative demands since rainfall onset are met, and there is sufficient infiltration for the  
114 wetting-front to arrive at the sensor. Rainfall events large enough to induce a soil moisture  
115 change ( $\Delta\theta$ ) are evident as a rainfall threshold in the relationship between  $P$  and  $\Delta\theta$ . An example  
116 time series of  $P$  and  $\theta$  (Fig. 1b) yields a  $P$  versus  $\Delta\theta$  relationship (Fig. 1c) with clear threshold

117 behavior. There are multiple equations whose functional forms allow for extraction of this  
 118 threshold; here we express this relationship as:

$$119 \quad P = \frac{a}{(1+b \cdot \exp(-c \cdot \Delta\theta))} \quad (1)$$

120 where  $P$  is the total rainfall event depth,  $\Delta\theta$  is the corresponding soil moisture change, and  $a$ ,  $b$ ,  
 121 and  $c$  are fitted parameters. Figure 2 illustrates this relationship and model fitting for observed  
 122  $\Delta\theta$  data from six plots at one of our study sites described below. The y-intercept of Eq. 1 (i.e.,  
 123 where  $\Delta\theta$  departs from zero) is given by:

$$124 \quad P_s = \frac{a}{(1+b)} \quad (2)$$

125 where  $P_s$  represents the total rainfall required to saturate  $\beta_s$ , meet evaporative demands between  
 126 storm onset and observed  $\Delta\theta$ , and supply any infiltration required to induce soil moisture  
 127 response once  $\beta_s$  has been saturated. This equality can be expressed as:

$$128 \quad P_s = \beta_s + \int_0^T E dt + \int_t^T f dt = \beta_s + \int_0^t E dt + \int_t^T E dt + \int_t^T f dt \quad (3)$$

129 where  $T$  is the total time from rainfall onset until observed change in  $\theta$  (i.e., the wetting front  
 130 arrival),  $t$  is the time when  $\beta_s$  is satisfied, and  $E$  and  $f$  are the evaporation and infiltration rates,  
 131 respectively. To connect this empirical observation to existing analytical frameworks [g., *Gash*  
 132 1979], we adopt the term  $P_G$ , defined as the rainfall depth needed to saturate  $\beta_s$  and supply  
 133 evaporative losses between rainfall onset (time = 0) and  $\beta_s$  saturation (time =  $t$ ):

$$134 \quad P_G = \beta_s + \int_0^t E dt \quad (4)$$

135 Solving for  $\beta_s$  in Eq. 3 and substituting into Eq. 4 yields:

$$136 \quad P_G = P_s - \int_t^T E dt - \int_t^T f dt \quad (5)$$

137 Equation 5 may be simplified by assuming that average infiltration and evaporation rates apply  
 138 during the relatively short period between  $t$  and  $T$ , such that:

139  $P_G = P_s - \bar{f}(T - t) - \bar{E}(T - t)$  (6)

140 where  $\bar{f}$  is the average soil infiltration rate and  $\bar{E}$  is the average rate of evaporation from the  
 141 forest surface (i.e., canopy, groundcover, and soil) during the time from  $t$  to  $T$  [see *Gash*, 1979].

142 The storage capacity  $\beta_s$  can now be calculated following *Gash* [1979] as:

143 
$$\beta_s = -\frac{\bar{E}}{\bar{P}} \frac{P_G}{\ln(1-\frac{\bar{E}}{\bar{P}})} = -\frac{\bar{E}}{\bar{P}} \frac{[P_s - (T-t)(\bar{f} + \bar{E})]}{\ln(1-\frac{\bar{E}}{\bar{P}})}$$
 (7)

144 where  $\bar{P}$  is the average rainfall rate and all other variables are as previously defined. In Eq. 5,  $\bar{E}$   
 145 is usually estimated using the Penman-Monteith equation [*Monteith*, 1965], setting canopy  
 146 resistance to zero (e.g., *Ghimire et al.*, 2017).

147 A key challenge in applying Eq. 5, and thus for the overall approach, is quantifying  
 148 infiltration, since the time,  $t$ , when  $\beta_s$  is satisfied is unknown. Moreover, the infiltration rate  
 149 embedded in  $P_s$  is controlled by  $\bar{P}$  and initial soil moisture content ( $\theta_i$ ). It is worth noting that  
 150 shallower sensor depth placement would likely eliminate the need for this step (see Discussion).  
 151 However, to overcome this limitation in our study (where our soil moisture sensor was 15 cm  
 152 below the ground surface), we used the 1-D unsaturated flow model HYDRUS-1D [*Simunek et*  
 153 *al.*, 1995] to simulate the required time for the wetting front to arrive ( $T_w$ ) at the sensor under  
 154 bare soil conditions across many combinations of  $\bar{P}$  and  $\theta_i$ . As such,  $T_w$  represents the time  
 155 required for a soil moisture pulse to reach the sensor once infiltration begins (i.e., after  $\beta_s$  has  
 156 been filled), which is  $T - t$  in Eq. 7. For each simulation,  $T_w$  (signaled by the first change in  $\theta$  at  
 157 sensor depth) was recorded and used to develop a statistical model of  $T_w$  as a function of  $\bar{P}$  and  $\theta_i$ .  
 158 We used plot-specific soil moisture retention parameters from Florida Soil Characterization  
 159 Retrieval System (<https://soils.ifas.ufl.edu/flsoils/>) to develop these curves for our sites, but  
 160 simulations can be applied for any soil with known or estimated parameters.

161 Simulations revealed that  $T_w$  at a specific depth declined exponentially with increasing  $\theta_i$ :

$$162 \quad T_w = ae^{-b\theta_i} \quad (8)$$

163 where  $a$  and  $b$  are fitting parameters. Moreover, the parameters  $a$  and  $b$  in Eq. (6) are well fitted  
164 by a power function of  $\bar{P}$ :

$$165 \quad a = a_1\bar{P}^{a_2}, b = b_1\bar{P}^{b_2} \quad (9)$$

166 where  $a_1$  and  $b_1$  are fitting parameters. These relationships are illustrated in Fig. 3 for a loamy  
167 sand across a range of  $\bar{P}$  and  $\theta_i$  at 15 cm depth. The relationship between  $\theta_i$  and  $T_w$  is very strong  
168 for small to moderate  $\bar{P}$  ( $< 3.0$  cm/hr). At higher values of  $\bar{P}$ ,  $T_w$  is smaller than the 15-minute  
169 sampling resolution, and these events were excluded from our analysis (see below).

170 Assuming that  $\bar{f}$  equals  $\bar{P}$  over the initial infiltration period from  $t$  to  $T$  (robust for most  
171 soils, see below), Eq. 7 can be modified to:

$$172 \quad \beta_s = \frac{-\bar{E}}{\bar{P}} \left[ \frac{P_s - T_w(\bar{P} + \bar{E})}{\ln\left(1 - \frac{\bar{E}}{\bar{P}}\right)} \right] \quad (10)$$

173 This approach assumes no surface runoff or lateral soil-water flow near the top of the soil profile  
174 from time  $t$  to  $T$ . Except for very fine soils under extremely high  $\bar{P}$ , this assumption generally  
175 holds during early storm phases, before ponding occurs [Mein and Larsen, 1973]. However,  
176 where strong layering occurs near the surface, lateral flow above the sensor (i.e., at capillary  
177 barriers or differential conductivity layers; Blume *et al.*, 2009) may occur, and wetting front  
178 simulations described above would need to account for layered soil structure to avoid potential  
179 overestimation of interception. Lateral flow within the duff layer during high-intensity  
180 precipitation events as observed by Blume *et al.* (2008) would be more difficult to correct for,  
181 though we note that since our goal is to determine  $\beta_s$ , extreme storms can be omitted from the  
182 analysis when implementing Eqs. 1-10, without compromising  $\beta_s$  estimates. Similarly, not  
183 accounting for the presence of preferential flow (e.g., finger flow, funnel flow, or macropore



184 flow; *Orozco-Lopez et al.*, 2018) in wetting front calculations could lead to underestimation of  
 185 interception, though application in coarser texture soils (as evaluated here) likely minimize this  
 186 challenge. More generally, these limitations can be minimized by placing the soil moisture  
 187 sensor close to the soil surface (e.g., within 5 cm). Finally, we note that values of  $\beta_s$  from Eq. 10  
 188 represent combined interception from canopy and groundcover, but the method does not allow  
 189 for disaggregation of these two components.

### 190 **Calculating Interception**

191 Interception storage and subsequent evaporation (sometimes referred to as interception  
 192 loss) for a given rain event are driven by both antecedent rain (which fills storage) and  
 193 evaporation (which depletes it). Instantaneous available storage ranges from zero (saturated) to  
 194 the maximum capacity (i.e.,  $\beta_s$  which occurs when the storage is empty). While discrete, event-  
 195 based interception models [*Gash*, 1979, 1995; *Liu*, 1998] have been widely applied to estimate  
 196 interception, continuous models more accurately represent time-varying dynamics in interception  
 197 storage and losses. We adopted the continuous, physically based interception modeling  
 198 framework of *Liu* [1998, 2001]:

$$199 \quad I = \beta_s(D_0 - D) + \int_0^t (1 - D)E dt \quad (11)$$

200 where  $I$  is interception,  $D_0$  is the forest dryness index at the beginning of the time step  $t$ ,  $D$  is the  
 201 forest dryness index at time the end of  $t$ , and  $E$  is the evaporation rate from wetted surfaces. The  
 202 dryness index at each time-step is calculated as:

$$203 \quad D = 1 - \frac{C}{\beta_s} \quad (12)$$

204 where  $C$  is “adherent storage” (i.e., water that does not drip to the ground) and is given by:

$$205 \quad C = \beta_s \left( 1 - D_0 \exp\left(\frac{-(1-\tau)P}{\beta_s}\right) \right) \quad (13)$$

206 where  $\tau$  is the free throughfall coefficient. Because our formulation of  $\beta_s$  in Eq. 10 incorporates  
207 both canopy and groundcover components (i.e., negligible true throughfall), we approximated  $\tau$   
208 in Eq. 13 as zero. Between rainfall events, water in interception storage evaporates to meet  
209 atmospheric demand, until the dryness index,  $D$  reaches unity [Liu 1997]. The rate of  
210 evaporation from wetted surfaces between rainfall events ( $E_s$ ) is:

$$211 \quad E_s = E(1 - D)\exp\left(\frac{E}{\beta_s}\right) \quad (14)$$

212 A numerical version of Eq. 11 to calculate interception at each time step,  $t$ , is expressed as:

$$213 \quad I = \beta_s(D_{t-1} - D_t) + \frac{1}{2}[E_{t-1}(1 - D_{t-1}) + E_t(1 - D_t)] \quad (15)$$

214 Eq. 15 quantifies continuous and cumulative interception using precipitation and other climate  
215 data (for  $E$ ) along with  $\beta_s$  derived from soil moisture measurements and corresponding  
216 meteorological data.

## 217 **Study Area and Data Collection**

218 As part of a multi-year study quantifying forest water use under varying silvicultural  
219 management, we instrumented six sites across Florida, each with six 2-ha plots spanning a wide  
220 range of forest structural characteristics. Data from two of the plots at one site were not used here  
221 due to consistent surface water inundation, yielding a total of 34 experimental forest plots. Sites  
222 varied in hydroclimatic forcing (annual precipitation range: 131 to 154 cm/yr and potential  $ET$   
223 range: 127 to 158 cm/yr) and hydrogeologic setting (shallow vs. deep groundwater table).  
224 Experimental plots within sites varied in tree species, age, density, leaf area index (LAI),  
225 groundcover vegetation density (%GC), soil type, and management history (Table 1). Each site  
226 contained a recent clear-cut plot, a mature pine plantation plot, and a restored longleaf pine  
227 (*Pinus palustris*) plot; the three remaining plots at each site included stands of slash pine (*Pinus*  
228 *elliottii*), sand pine (*Pinus clausa*), or loblolly pine (*Pinus taeda*) subjected to varying

229 silvicultural treatments (understory management, canopy thinning, prescribed burning) and  
230 hardwood encroachment. The scope of the overall project (34 plots spanning 6 sites across  
231 Florida) and the emphasis on measuring variation in forest ET and water yield precluded  
232 conventional measurements of interception (e.g., throughfall and stemflow collectors). Because  
233 model estimates of interception were considered sufficient for water yield predictions across  
234 sites, the analyses presented here represent a proposal for additional insights about interception  
235 that can be gleaned from time series of soil moisture rather than a meticulous comparison of  
236 methods. We assessed results from this new proposed method using comparisons with numerous  
237 previous interception studies in pine stands in the southeastern US and elsewhere, and by testing  
238 for the expected associations between estimated interception and stand structure (e.g., LAI and  
239 groundcover).

240         Within each plot, three sets of TDR sensors (CS655, Campbell Scientific, Logan, UT,  
241 USA) were installed to measure soil moisture at multiple soil depths (Fig. 1a). Only data from  
242 the top-most sensor (15 cm below the ground surface) were used in this study. Soil-moisture  
243 sensors were located to capture representative variation in stand geometry and structure (i.e.,  
244 within and between tree rows) to capture variation in surface soil moisture response to rainfall  
245 events. While this spatial layout was intended to characterize the range of plot-scale forest  
246 canopy and groundcover heterogeneity, the three measurements locations were within a 10-m  
247 radius and thus represent localized (sub-plot) interception estimates. Within each clear-cut plot at  
248 each site, meteorological data (rainfall, air temperature, relative humidity, solar insolation, wind  
249 speed and direction) were measured using a weather station (GRSW100, Campbell Scientific,  
250 Logan, UT; Fig. 4c) every 3 seconds and used to calculate hourly  $E$  by setting the canopy  
251 resistance to zero [Ghimire *et al.*, 2017; Gash, 1995; Monteith, 1965]. Growing season forest

252 canopy LAI ( $m^2 m^{-2}$ ) and groundcover (%) were measured at every 5-m node within a 50 m x 50  
253 m grid surrounding soil moisture measurement banks. LAI was measured at a height of 1 m  
254 using a LI-COR LAI-2200 plant canopy analyzer, and %GC was measured using a 1  $m^2$  quadrat.

255 To estimate  $\beta_s$ , mean  $\Delta\theta$  values from the three surface sensors were calculated for all  
256 rainfall events separated by at least 72 hours. Storm separation was necessary to ensure the  
257 canopy and groundcover surfaces were mostly dry (and thus antecedent storage capacity =  $\beta_s$ ) at  
258 the onset of each included rainfall event. Rainfall events were binned into discrete classes by  
259 depth and plotted against mean  $\Delta\theta$  to empirically estimate  $P_s$  (e.g., Fig. 2). For each rainfall bin,  
260 mean  $\theta_i$ ,  $\bar{P}$  and  $\bar{E}$  were also calculated to use in Eq. 10, which was then applied to calculate  $\beta_s$ .  
261 Subsequently, we developed generalized linear models (GLMs) using forest canopy structure  
262 (site-mean LAI), mean groundcover (% GC), hydrogeologic setting (shallow vs. deep  
263 groundwater table), and site as potential predictors, along with their interactions, to statistically  
264 assess predictors of  $\beta_s$  estimates. Because models differed in fitted parameter number, the best  
265 model was selected using the Akaike Information Criteria (AIC; Akaike, 1974). Finally, we  
266 calculated cumulative annual interception ( $I_a$ ) and its proportion of total precipitation ( $I_a/P$ ) for  
267 each study plot using the mean  $\beta_s$  for each plot (across the 3 sensor banks), climate data from  
268 2014 to 2016, and Eq. 15. Differences in  $I_a/P$  across sites and among plots within sites were  
269 assessed using ANOVAs. All analyses were performed using R [R Core Team, 2017].

270

## 271 **Results**

### 272 **Total Storage Capacity ( $\beta_s$ )**

273 The exponential function used to describe the  $P$ - $\Delta\theta$  relationship (Eq. 1) showed strong  
274 agreement with observations at all sites and plots (overall  $R_2 = 0.80$ ;  $0.47 \leq R_2 \leq 0.97$ ; Table 1)

275 as illustrated for a single site in Fig. 2. This consistency across plots and sites suggests that Eq. 1  
276 is capable of adequately describing observed  $P-\Delta\theta$  relationships, enabling estimates of  $\beta_s$  across  
277 diverse hydroclimatic settings and forest structural variation. Estimates of  $\beta_s$  ranged from 0.01 to  
278 0.62 cm, with a mean of 0.30 cm (Table 1). Plot-scale LAI was moderately correlated with plot-  
279 mean  $\beta_s$ , describing roughly 32% of observed variation across plots (Fig. 4a). This relatively  
280 weak association may arise because LAI measurements only characterize canopy cover, while  $\beta_s$   
281 combines canopy and groundcover storage. The best GLM of  $\beta_s$  (Fig. 4b) used %GC and an  
282 interaction term between site and LAI ( $R^2 = 0.84$  and  $AIC = 253.7$ , Table 2). The best GLM  
283 without site used LAI and hydrogeologic setting (shallow vs. deep water table) but had reduced  
284 performance ( $R^2 = 0.55$  and  $AIC = 338.3$ ; Table 2). All models excluding LAI as a predictor  
285 performed poorly, so we report model comparisons only for those including LAI.

### 286 **Annual Interception ( $I_a$ )**

287         Despite having similar rainfall regimes (mean annual precipitation ranging from 131 to  
288 154 cm yr<sup>-1</sup> across sites), mean annual interception ( $I_a$ ) differed significantly both across sites  
289 (one-way ANOVA  $p < 0.001$ ) and among plots within sites (one-way ANOVA  $p < 0.001$ ).  
290 Estimates of  $I_a/P$  across all plots and sites ranged from 6 to 21% of annual rainfall (Table 1) and  
291 were moderately, but significantly, correlated with mean LAI, explaining approximately 30% of  
292 variation in  $I_a/P$  (Fig. 5a). Correlations among  $I_a/P$  and LAI were stronger for individual sites  
293 than the global relationship ( $0.51 \leq R^2 \leq 0.84$ ), except for site EF, where  $I_a$  was small and similar  
294 across plots regardless of LAI (Fig. 5b; Table 1). This suggests that additional site-level  
295 differences (e.g., hydroclimate, soils, geology) play a role in driving  $I_a$ , as expected following  
296 from their effects on  $\beta_s$  described above.

297

## Discussion

298

299

300

301

302

303

304

305

306

307

308

309

310

311

312

313

314

315

316

317

318

319

When combined with local rainfall data, near-surface soil moisture dynamics inherently contain information about rainfall interception by above-ground structures. Using soil moisture data, we developed and tested an analytical approach for estimating total interception storage capacity ( $\beta_s$ ) that includes canopy, understory, and groundcover vegetation, as well as any litter on the forest floor. The range of  $\beta_s$  given by our analysis (mean  $\beta_s = 0.30$  cm;  $0.01 \leq \beta_s \leq 0.62$  cm) is close to, but generally higher than previously reported canopy-only storage capacity values for similar pine forests (e.g., 0.17 to 0.20 cm for mature southeastern USA pine forests; *Bryant et al.* 2005). Moreover, our estimates of  $\beta_s$  and annual interception corresponded to expected forest structure controls (e.g., LAI and ground cover) on interception, further supporting the feasibility of the soil moisture-based approach. However, we emphasize that a more robust validation of the method using co-located and contemporaneous measurement using standard techniques is warranted. Below we summarize the assumptions and methodological considerations that affect the potential utility and limitation of the method.

An important distinction between our proposed method and previous interception measurement approaches is that the soil moisture-based method estimates composite rainfall interception of not only the canopy, but also of the groundcover vegetation and forest floor litter. Rainfall storage and subsequent evaporation from groundcover vegetation and litter layers can be as high, or higher than, canopy storage in many forest landscapes [*Putuhena and Cordery*, 1996; *Gerrits et al.*, 2010]. For example, *Li et al.* [2017] found that the storage capacity of a pine forest floor in China was between 0.3 and 0.5 cm, while maximum canopy storage was  $< 0.1$  cm. *Putuhena and Cordery* [1996] also estimated storage capacity of pine forest litter to be approximately 0.3 cm based on direct field measurements. *Gerrits et al.* [2007] found forest floor

320 interception to be 34% of measured precipitation in a beech forest, while other studies have  
321 shown that interception by litter can range from 8 to 18% of total rainfall [*Gerrits et al.*, 2010;  
322 *Tsiko et al.*, 2012; *Miller et al.*, 1990; *Pathak et al.*, 1985; *Kelliher et al.*, 1992]. A recent study  
323 using leaf wetness observations [*Acharya et al.*, 2017] found the storage capacity of eastern  
324 redcedar (*Juniperus virginiana*) forest litter to range from 0.12 to as high as 1.12 cm, with forest  
325 litter intercepting approximately 8% of gross rainfall over a six-month period. Given the  
326 composite nature of forest interception storage and the range of storage capacities reported in  
327 these studies, the values we report appear to be plausible and consistent with the expected  
328 differences between canopy-only and total interception storage.

329         Interception varies spatially and temporally and is driven by both  $\beta_s$  and climatic  
330 variation (i.e.,  $P$  and  $E$ ). Our approach represents storage dynamics by combining empirically  
331 derived  $\beta_s$  estimates with climatic data using a previously developed continuous interception  
332 model [*Liu* 1998, 2001]. Cumulative  $I_a$  estimates in this study ranged considerably (i.e., from 6%  
333 to 21% of annual rainfall) across the 34 plots, which were characterized by variation in canopy  
334 structure ( $0.12 < LAI < 3.70$ ) and groundcover ( $7.9 < \%GC < 86.2$ ). In comparison, interception  
335 by pine forests reported in the literature (all of which report either canopy-only or groundcover-  
336 only values, but not their composite) range from 12 to 49% of incoming rainfall [*Bryant et al.*,  
337 2005; *Llorens et al.*, 1997; *Kelliher and Whitehead*, 1992; *Crockford and Richardson*, 1990].  
338 Notably, most of the variation in this range is driven by climate rather than forest structure, with  
339 the highest  $I_a$  values from more arid regions [e.g., *Llorens et al.* 1997]. Future work could also  
340 consider seasonally disaggregated measurements to explore intra-annual variation in canopy  
341 structure and litter composition [*Van Stan et al.* 2017].

342 Broad agreement between our results and literature  $I_a$  values again supports the potential  
343 utility of our method for estimating this difficult-to-measure component of the water budget,  
344 though additional direct comparisons would further support this assertion. Additionally, the  
345 magnitude and heterogeneity of our  $I_a$  estimates across a single forest type (southeastern US  
346 pine) underscores the urgent need for empirical measurements of interception that incorporate  
347 information on both canopy and groundcover storage in order to develop accurate water budgets.  
348 This conclusion is further bolstered by the persistent importance of site-level statistical effects in  
349 predicting  $\beta_s$  (and therefore  $I_a$ ), even after accounting for forest structural attributes, which  
350 suggests there are influential edaphic or structural attributes that we are not currently adequately  
351 assessing. For example, while estimated  $I_a$  in clear-cut plots was generally smaller than plots  
352 with a developed canopy, as expected, one exception was at EF where the clear-cut plot  
353 exhibited the highest  $I_a$  of the six EF plots (8.4%, Table 1). However, differences among all EF  
354 plots were very small ( $I_a$  ranged only from 7.9 to 8.4 % of annual rainfall), a rate consistent with  
355 or even lower than other clear cuts across the study. This site is extremely well drained with  
356 nutrient-poor sandy soils and differs from other sites in that it has dense litter dominated by  
357 mosses, highlighting the need for additional local measurements to better understand how forest  
358 structure controls observed interception.

359 There are several important methodological considerations and assumptions inherent to  
360 estimating interception using near-surface soil moisture data. First is the depth at which soil  
361 moisture is measured. Ideally,  $\theta$  would be measured a few centimeters into the soil profile,  
362 eliminating the need to account for infiltration when calculating  $P_G$  in Eqs. (4-6) and thereby  
363 alleviating concerns about lateral and preferential flow. Soil moisture data used here were  
364 leveraged from a study of forest water yield, with sensor deployment depths selected to



365 efficiently integrate soil moisture patterns through the vadose zone. The extra step of modeling  
366 infiltration likely increases uncertainty in  $\beta_s$  given field-scale heterogeneity in soil properties and  
367 potential lateral and preferential flow. Specifically, lateral flow would delay wetting-front  
368 arrival, leading to overestimation of interception, while preferential flow would do the opposite.  
369 Despite these caveats, infiltration in our system was extremely well-described using wetting  
370 front simulations of arrival time based on initial soil moisture and rainfall. As such, while we  
371 advocate for shallower sensor installation and direct comparison to standard methods in future  
372 efforts, the results presented here given the available sensor depth seem tenable for this and other  
373 similar data sets.

374 Another methodological consideration is that, in contrast to the original Gash (1979)  
375 formulation, Eq. 5 does not explicitly include throughfall. While throughfall has been a critical  
376 consideration for rainfall partitioning by the forest canopy, our approach considers total  
377 interception by aboveground forest structures (canopy, groundcover, and litter). A portion of  
378 canopy throughfall is captured by non-canopy storage and thus intercepted. Constraining this  
379 fraction is not possible with the data available, and indeed our soil moisture response reflects the  
380 “throughfall” passing the canopy, understory and litter. Similarly, estimation of  $\beta_s$  using Eqs. 1-7  
381 cannot directly account for stemflow, which can be an important component of rainfall  
382 partitioning in forests [e.g., *Bryant et al.*, 2005]. We used the mean soil moisture response across  
383 three sensor locations (close to a tree, away from the tree but below the canopy, and within inter-  
384 canopy rows), which lessens the impact of this assumption on our estimates of  $\beta_s$ . Further, Eqs.  
385 (3-10) assume the same evaporation rate,  $E$ , for intercepted water from the canopy and from the  
386 understory. Evaporation rates may vary substantially between the canopy, understory, and forest  
387 floor [*Gerrits et al.*, 2007, 2010], especially in more energy-limited environments. Future work

388 should consider differential evaporation rates within each interception storage, particularly since  
389 the inclusion of litter as a component potentially accentuates these contrasts in  $E$ .

390         Among the many challenges of measuring interception is the spatial heterogeneity of  
391 canopy and ground cover layers, with associated heterogeneity in interception rates. Our study  
392 deployed only three sensors per plot, yielding interception estimates that covaried with the  
393 expected forest structure controls (i.e., LAI and ground cover) and that aligned closely with  
394 literature reported values. Nonetheless, future work should assess spatial variation in soil  
395 moisture responses to known heterogeneity in net precipitation (i.e., throughfall plus stemflow)  
396 across forest stands (e.g., *Roth et al.*, 2007; *Wullaert et al.*, 2009; *Fathizadeh et al.*, 2014). Soil  
397 moisture responses are likely driven by variation in both vegetation and soil properties [*Metzger*  
398 *et al.*, 2017], indicating the need for future inquiry across systems to inform the number and  
399 locations of soil moisture sensor needed for accurate interception estimates in a variety of  
400 settings. Notably, the requisite sampling frequency for aboveground interception is estimated to  
401 be 25 funnel collectors per hectare (or more) to maintain relative error below 10% for long-term  
402 monitoring, with as many as 200 collectors needed for similar error rates during individual event  
403 sampling [*Zimmerman et al.*, 2010; *Zimmerman and Zimmerman*, 2014]. Spatial averaging using  
404 larger trough collectors reduces some of this sampling effort, yielding guidance of 5 trough  
405 collectors per hectare for assessment of multiple precipitation events or up to 20 per hectare for  
406 individual events [*Zimmerman and Zimmerman*, 2014].

407         While the comparative spatial integration extent of aboveground collectors versus soil  
408 moisture sensors remains unknown, the strong correspondence between our measurements and  
409 literature reported values for the magnitude of interception storage, as well as the forest structure  
410 controls (i.e., LAI and ground cover) on that storage volume, underscores that soil moisture

411 measurements, at least in this setting, can integrate key quantitative aspects of the interception  
412 process. One possible explanation for the consistency of our results with previous interception  
413 studies using aboveground collectors is that soil moisture averages across extant spatial  
414 heterogeneity in canopy processes, providing comparable spatial integration to throughfall  
415 troughs. In this context, soil moisture measurements have several operational advantages over  
416 trough-type collectors, including automated data logging and reduced maintenance burden (e.g.,  
417 clearing litter accumulation in collectors), while also providing total interception estimates (as  
418 opposed to canopy-only measures). Additional soil moisture measurements would undoubtedly  
419 improve the accuracy of these estimates, and indeed we recommend that more direct  
420 methodological comparisons are needed to determine the optimal number of sensors for future  
421 applications. Overall, however, our results support the general applicability of this proposed soil  
422 moisture-based approach for developing “whole-forest” interception estimates across a wide  
423 range of hydroclimatic and forest structural settings.

424

425

## Conclusions

426

427

428

429

430

431

432

433

Rainfall interception by forests is a dynamic process that is strongly influenced by  
rainfall patterns (e.g., frequency, intensity), along with various forest structural attributes such as  
interception storage capacity ( $\beta_s$ ) [Gerrits *et al.*, 2010]. In this work, we coupled estimation of a  
total (or “whole-forest”)  $\beta_s$  parameter with a continuous water balance model [Liu, 1997, 2001;  
*Rutter et al.*, 1975], providing an integrative approach for quantifying time-varying and  
cumulative interception. We propose that soil moisture-based estimates of  $\beta_s$  have the potential  
to more easily and appropriately represent combined forest interception relative to existing time-  
and labor-intensive field methods that fail to account for groundcover and litter interception.

434 However, we emphasize that further experimental work is needed to validate this promising  
435 approach. Soil moisture can be measured relatively inexpensively and easily using continuous  
436 logging sensors that require little field maintenance, facilitating application of the presented  
437 approach across large spatial and temporal extents and reducing the time and resources that are  
438 needed for other empirical measures [e.g., *Lundberg et al.*, 1997]. Finally, while our comparisons  
439 with other empirical measures of forest canopy interception should be treated cautiously, this  
440 approach yields values that are broadly consistent with the literature and provide an estimate of  
441 combined canopy and groundcover storage capacity that has the potential to improve the  
442 accuracy of water balances models at scales from the soil column to watershed.

443

444

#### References

- 445 Acharya, B.S., Stebler, E., and Zou, C.B.: Monitoring litter interception of rainfall using leaf  
446 wetness sensor under controlled and field conditions. *Hydrological Processes*, 31, 240-  
447 249: DOI: 10.1002/hyp.11047, 2005
- 448 Benyon, R.G., Doody, and T. M.: Comparison of interception, forest floor evaporation and  
449 transpiration in *Pinus radiata* and *Eucalyptus globulus* plantations. *Hydrological*  
450 *Processes* **29** (6): 1173–1187 DOI: 10.1002/hyp.10237, 2015
- 451 Blume, T., Zehe, E. and Bronstert, A.: Use of soil moisture dynamics and patterns at different  
452 spatio-temporal scales for the investigation of subsurface flow processes. *Hydrology and*  
453 *Earth System Sciences*, **13**(7): 1215-1233, 2009
- 454 Blume, T., Zehe, E., and Bronstert, A. : Investigation of runoff generation in a pristine, poorly  
455 gauged catchment in the Chilean An- des. II: Qualitative and quantitative use of tracers  
456 at three differ- ent spatial scales. *Hydrol. Proc.*, **22**: 3676–3688, 2008
- 457 Bryant, M.L., Bhat, S., and Jacobs, J.M.: Measurements and modeling of throughfall variability  
458 for five forest communities in the southeastern US. *Journal of Hydrology*, DOI:  
459 10.1016/j.jhydrol.2005.02.012, 2005
- 460 Bulcock, H.H., and Jewitt, G.P.W.: Modelling canopy and litter interception in commercial  
461 forest plantations in South Africa using the Variable Storage Gash model and idealized  
462 drying curves. *Hydrol. Earth Syst. Sci* **16**: 4693–4705 DOI: 10.5194/hess-16-4693-2012,  
463 2012

- 464 Calder, I. R.: A stochastic model of rainfall interception. *Journal of Hydrology*, **89**: 65-71, doi:  
465 10.1016/0022-1694(86)90143-5, 1986
- 466 Calder, I.R.: Evaporation in the Uplands. Wiley, New York, pp. 148, 1990
- 467 Carlyle-Moses, D.E., and Gash, J.H.C.: Rainfall Interception Loss by Forest Canopies. In  
468 Carlyle-Moses and Tanaka (Eds), *Ecological Studies* 216. DOI: 10.1007/978-94-007-  
469 1363, 2011
- 470 Carlyle-Moses, D.E., and Price, A.G.: Modelling canopy interception loss from a Mediterranean  
471 pine-oak stand, northeastern Mexico. *Hydrological Processes* **21** (19): 2572–2580 DOI:  
472 10.1002/hyp.6790, 2007
- 473 Crockford, R.H., and Richardson, D.P.: Partitioning of rainfall into throughfall, stemflow and  
474 interception: effect of forest type, ground cover and climate. *Hydrological Processes* **14**  
475 (16–17): 2903–2920 DOI: 10.1002/1099-1085(200011/12)14:16/17<2903::AID-  
476 HYP126>3.0.CO;2-6, 2000
- 477 David, T. S., Gash, J.H. C., Valente, F., Pereira, J. S., Ferreira, M.I. and David, J. S.:  
478 Rainfall interception by an isolated evergreen oak tree in aMediterranean  
479 savannah.*Hydrological Processes* **20**: 2713–2726. DOI: 10.1002/hyp.6062,  
480 2006
- 481 Fathizadeh, O., Attarod, P., Keim, R.F., Stein, A., Amiri, G.Z. and Darvishsefat, A.A., 2014.  
482 Spatial heterogeneity and temporal stability of throughfall under individual *Quercus*  
483 *brantii* trees. *Hydrological Processes*, 28(3), pp.1124-1136.
- 484 Gash, J.H.C., Lloyd, C.R., and Lachaud, B. G.: Estimating sparse forest rainfall interception with  
485 an analytical model. *Journal of Hydrology* **170**: 79–86, 1995
- 486 Gash, J.H.C.: An analytical model of rainfall interception by forests. *Quarterly Journal of the*  
487 *Royal Meteorological Society* **105** (443): 43–55 DOI: 10.1002/qj.49710544304, 1979
- 488 Gerrits, A.M.J., Savenije, H.H.G., Hofmann, L., and Pfister, L.: New technique to measure forest  
489 floor interception – an application in a beech forest in Luxembourg. *Hydrol. Earth Syst.*  
490 *Sci* **11**: 695–701, 2007
- 491 Ghimire, C.P., Bruijnzeel, L.A., Lubczynski, M.W., and Bonell, M.: Rainfall interception by  
492 natural and planted forests in the Middle Mountains of Central Nepal. *Journal of*  
493 *Hydrology* **475**: 270–280 DOI: 10.1016/j.jhydrol.2012.09.051, 2012
- 494 Ghimire, C.P., Bruijnzell, L.A., Lubczynski, M.W., Ravelona, M., Zwartendijk, B.W., and  
495 Meervald, H.H.: Measurement and modeling of rainfall interception by two differently  
496 aged secondary forests in upland eastern Madagascar, *Journal of Hydrology*, DOI:  
497 10.1016/j.jhydrol.2016.10.032, 2017

- 498 Jarvis, N.J., Moeys, J. Koestel, J., and J.M. Hollis.: Preferential flow in a pedological  
 499 perspective. In: Lin, H. , editor, *Hydropedology: Synergistic integration of soil science*  
 500 *and hydrology*. Academic Press, Waltham, MA. p. 75–120. doi:10.1016/B978-0-12-  
 501 386941-8.00003-4, 2012.: Understanding preferential flow in the vadose zone: Recent  
 502 advances and future prospects. *Vadose Zone J.* **15** (12). doi:10.2136/vzj2016.09.0075,  
 503 2016
- 504 Kelliher, F.M., Whitehead, D., and Pollock D.S.: Rainfall interception by trees and slash in a  
 505 young *Pinus radiata* D. Don stand. *Journal of Hydrology* **131** (1–4): 187–204 DOI:  
 506 10.1016/0022-1694(92)90217-J, 1992
- 507 Li, X., Xiao, Q., Niu, J., Dymond, S., Mcherson, E. G., van Doorn, N., Yu, X., Xie, B., Zhang,  
 508 K., and Li, J.: Rainfall interception by tree crown and leaf litter: an interactive process.  
 509 *Hydrological Processes* DOI: 10.1002/hyp.11275, 2017
- 510 Liu, J.: A theoretical model of the process of rainfall interception in forest canopy. *Ecological*  
 511 *Modelling* **42**: 111–123, 1988
- 512 Liu, S.: A new model for the prediction of rainfall interception in forest canopies. *Ecological*  
 513 *Modelling* **99**: 15–159, 2001
- 514 Liu, S.: Estimation of rainfall storage capacity in the canopies of cypress wetlands and slash pine  
 515 uplands in North-Central Florida. *Journal of Hydrology* **207**: 32–41, 1998
- 516 Liu, S.: Evaluation of the Liu model for predicting rainfall interception in forests world-wide.  
 517 *Hydrological Processes* **15** (12): 2341–2360 DOI: 10.1002/hyp.264, 2001
- 518 Llorens, P., and Poch, R.: Rainfall interception by a *Pinus sylvestris* forest patch overgrown in a  
 519 Mediterranean mountainous abandoned area I. Monitoring design and results down to  
 520 the event scale. *Journal of Hydrology* **199**: 331–345, 1997
- 521 Lundberg, A., Eriksson, M., Halldin, S., Kellner, E., and Seibert, J.: New approach to the  
 522 measurement of interception evaporation. *Journal of Atmospheric and Oceanic*  
 523 *Technology* **14** (5), 1023–1035, 1997
- 524 Massman, W.J.: The derivation and validation of a new model for the interception of rainfall by  
 525 forests. *Agricultural and Forest Meteorology* **28**: 261–286, 1983
- 526 Merriam, R.A.: A note on the interception loss equation. *Journal of Geophysical Research* **65**  
 527 (11): 3850–3851 DOI 10.1029/JZ065i011p03850, 1960
- 528 Metzger, J.C., Wutzler, T., Dalla Valle, N., Filipzik, J., Grauer, C., Lehmann, R., Roggenbuck,  
 529 M., Schelhorn, D., Weckmüller, J., Küsel, K. and Totsche, K.U., 2017. Vegetation  
 530 impacts soil water content patterns by shaping canopy water fluxes and soil  
 531 properties. *Hydrological processes*, *31*(22), pp.3783-3795.

- 532 Muzylo, A., Llorens, P., Valente, F., Keizer, J.J., Domingo, F., and Gash, J.H.C. Gash. A review  
533 of rainfall interception modelling. *Journal of Hydrology* **370**: 191–206 DOI:  
534 10.1016/j.jhydrol.2009.02.058, 2009
- 535 Orozco-López, E., Muñoz-Carpena, R., Gao, B., and Fox, G.A.: Riparian vadose zone  
536 preferential flow: Review of concepts, limitations, and perspectives. *Vadose Zone*  
537 *Journal* **17**: doi: 10.2136/vzj2018.02.0031, 2018
- 538 Pook, E.W., Moore, P.H.R., and Hall, T.: Rainfall interception by trees of *Pinus radiata* and  
539 *Eucalyptus viminalis* in a 1300 mm rainfall area of southeastern New South Wales: I.  
540 Gross losses and their variability. *Hydrological Processes* **5** (2): 127–141 DOI:  
541 10.1002/hyp.3360050202, 1991
- 542 Putuhena, W.M., and Cordery, I.: Estimation of interception capacity of the forest floor. *Journal*  
543 *of Hydrology* **180**: 283–299, 1996
- 544 Roth, B.E., Slatton, K.C. and Cohen, M.J., 2007. On the potential for high-resolution lidar to  
545 improve rainfall interception estimates in forest ecosystems. *Frontiers in Ecology and*  
546 *the Environment*, 5(8), pp.421-428.
- 547 Rutter, A.J., Morton, A.J., and Robins, P.C.: A Predictive Model of Rainfall Interception in  
548 Forests. II. Generalization of the Model and Comparison with Observations in Some  
549 Coniferous and Hardwood Stands *Journal of Applied Ecology* **12** (1): 367–380, 1975
- 550 Savenije, H. H. G.: The importance of interception and why we should delete the term  
551 evapotranspiration from our vocabulary, *Hydrol. Processes*, 18, 1507 – 1511, 2004
- 552 Schaap, M.G., Bouten, W., and Verstraten, J.M.: Forest floor water content dynamics in a  
553 Douglas fir stand. *Journal of Hydrology* **201**: 367–383, 1997
- 554 Valente, F., David, J.S., and Gash, J.H.C.: Modelling interception loss for two sparse eucalypt  
555 and pine forests in central Portugal using reformulated Rutter and Gash analytical  
556 models. *Journal of Hydrology* **190**: 141–162, 1997
- 557 Van Dijk, A.I.J.M., and Bruijnzeel, L.A.: Modelling rainfall interception by vegetation of  
558 variable density using an adapted analytical model. Part 1. Model description. *Journal of*  
559 *Hydrology*, 247:230-238, 2001
- 560 Wei, Z., Yoshimura, K., Wang, L., Miralles, D.G., Jasechko, S., and Lee, X.: Revisiting the  
561 contribution of transpiration to global terrestrial evapotranspiration. *Geophysical*  
562 *Research Letters* **44** (6): 2792–2801 DOI: 10.1002/2016GL072235, 2017
- 563 Wullaert, H., Pohlert, T., Boy, J., Valarezo, C. and Wilcke, W., 2009. Spatial throughfall  
564 heterogeneity in a montane rain forest in Ecuador: extent, temporal stability and  
565 drivers. *Journal of Hydrology*, 377(1-2), pp.71-79.

566 Xiao, Q., McPherson, E.G., Ustin, S.L., and Grismer, M.E.: A new approach to modeling tree  
567 rainfall interception. *Journal of Geophysical Research: Atmospheres* **105** (D23): 29173–  
568 29188 DOI: 10.1029/2000JD900343, 2000

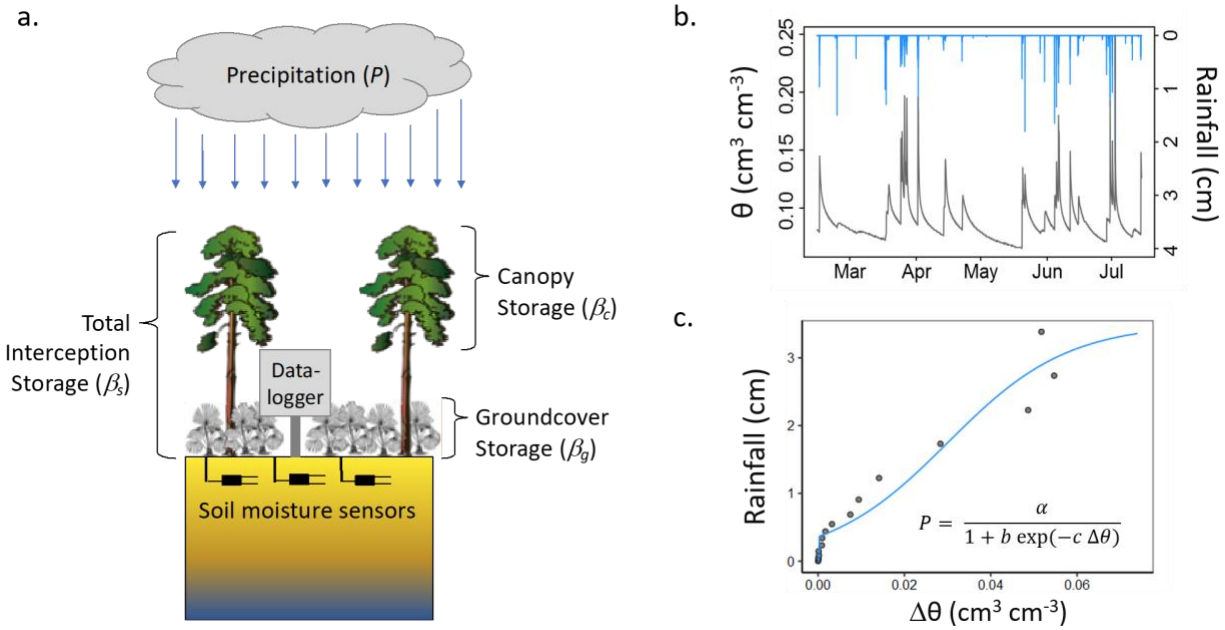
569 Zimmermann, A. and Zimmermann, B.: Requirements for throughfall monitoring: The roles of  
570 temporal scale and canopy complexity. *Agricultural and forest meteorology*, **189**, 125-  
571 139, 2014

572 Zimmermann, B., Zimmermann, A., Lark, R.M. and Elsenbeer, H.: Sampling procedures for  
573 throughfall monitoring: a simulation study. *Water Resources Research*, **46**(1): doi:  
574 10.1029/2009WR007776, 2010

575

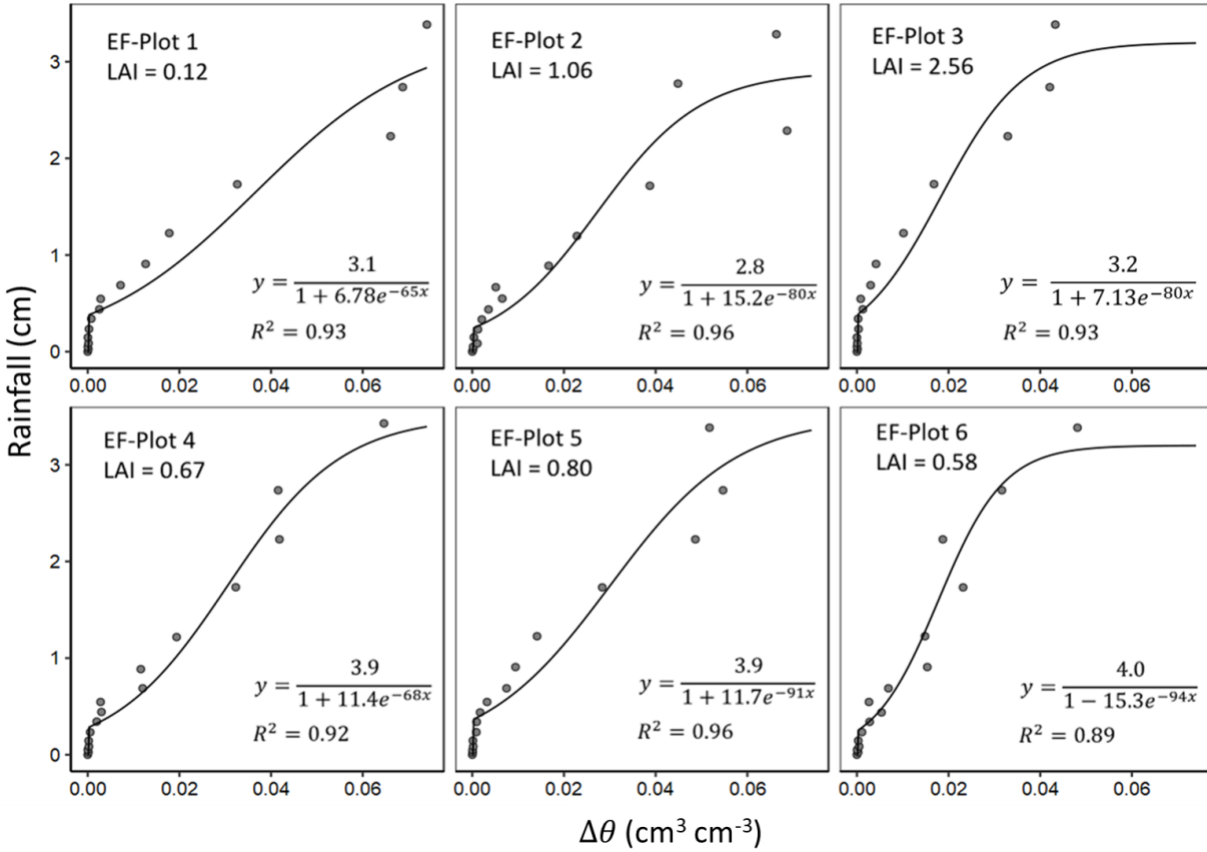
576





577

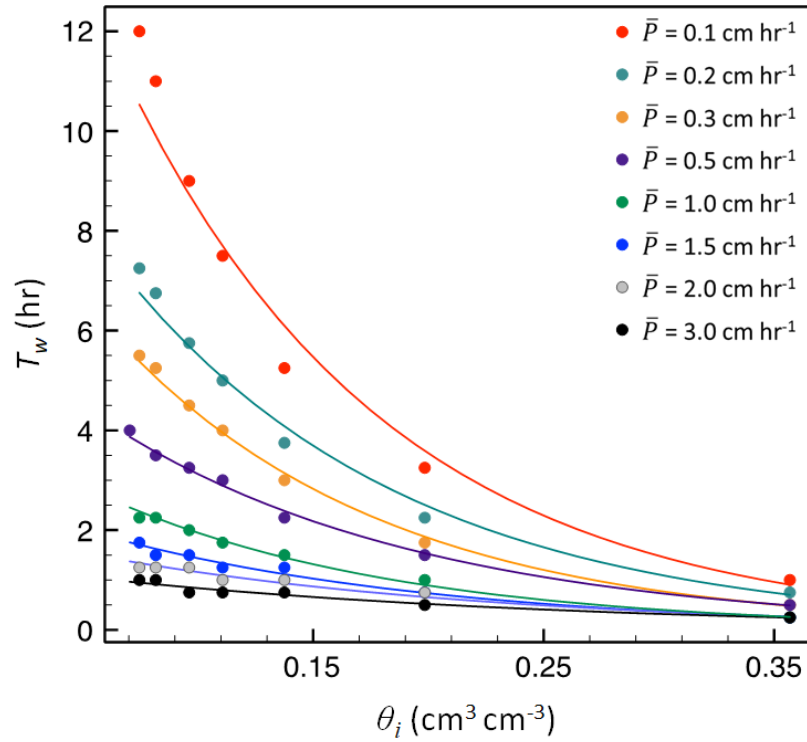
578 Figure 1. (a) Schematic illustration of experimental setup and interception water storages, where  
 579 total interception storage ( $\beta_s$ ) is the sum of canopy storage ( $\beta_c$ ) and groundcover (understory and  
 580 litter) storage ( $\beta_g$ ). (b) Example time series of rainfall (blue lines) and corresponding near-  
 581 surface soil moisture content ( $\theta$ , black line; observed at 15 cm in this study). (c) Resultant  
 582 relationship between rainfall and change in soil moisture  $\Delta\theta$  during rainfall, along with fitted  
 583 model to extract the y-intercept (i.e.,  $P_s$ ).



584

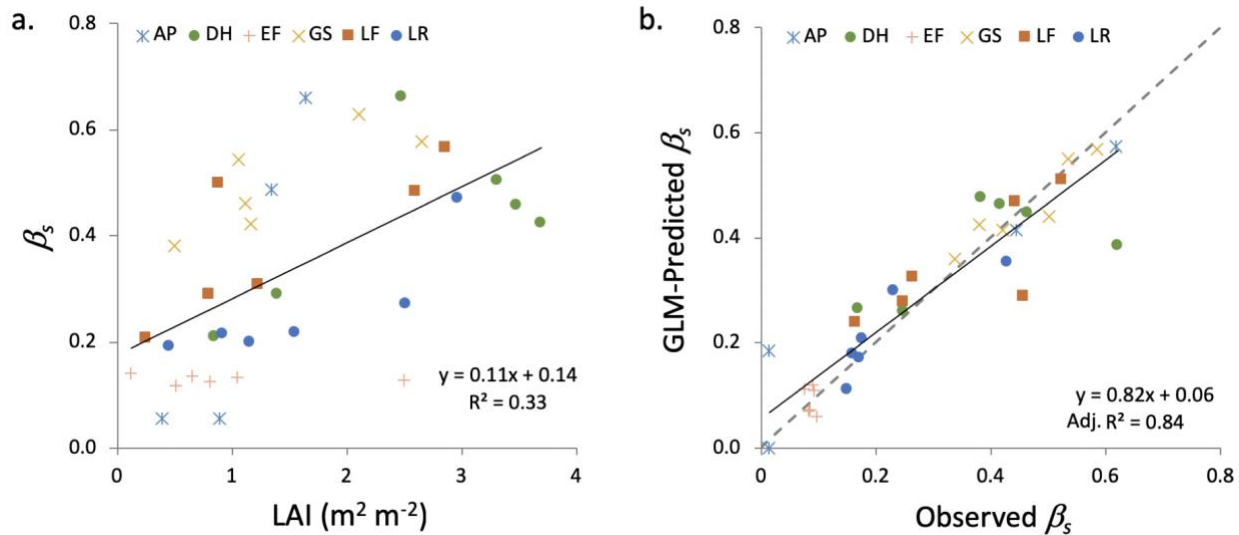
585 Figure 2: Binned rainfall depths vs change in soil moisture content ( $\Delta\theta$ ) for six plots at one of the  
 586 study sites used in the study (Econfina; EF). The y-intercept of the fitted relationships were used  
 587 to derive  $P_s$  in Eq. 2. Note different y-axis scale for EF-Plot 3.

588



589

590 Figure 3: Initial soil moisture content ( $\theta$ ) versus time of wetting front arrival ( $T_w$ ) at 15 cm depth  
 591 for a loamy sand soil. Dots are simulated results from HYDUS-1D simulation, and lines are the  
 592 exponential model given in Eq. 8, fitted for each rainfall rate,  $\bar{P}$ .



593

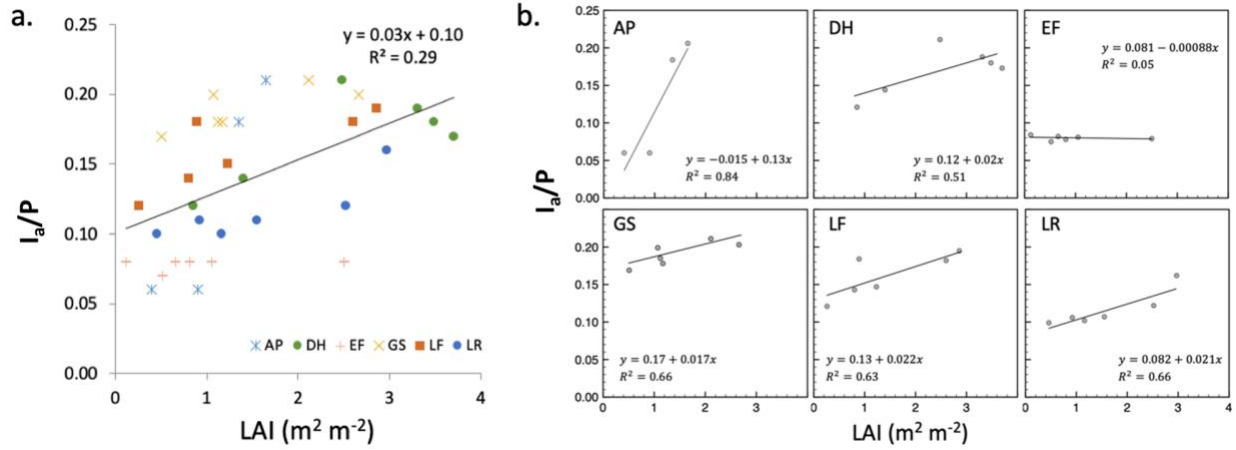
594 Figure 4. (a) Interception storage capacity ( $\beta_s$ ) versus leaf area index (LAI) for all sites and plots.

595 (b) Modeled versus observed  $\beta_s$  using the best GLM, which included % groundcover vegetation

596 and an interaction term between site and LAI. The dashed line is the 1:1 line.

597

598



599

600

601 Figure 5. (a) Annual proportion of rainfall that is intercepted ( $I_a/P$ ) intercepted versus LAI for all

602 sites and plots. (b) Site-specific  $I_a/P$  versus LAI relationships. The relationship is generally

603 strong except for the EF site, where the overall storage capacity is small across all values of LAI.

604

605 Table 1. Summary of storage capacity ( $\beta_s$ ) and annual interception losses ( $I_a$ ) for all sites and  
606 plots, along with plot characteristics (mean annual precipitation,  $P$ ; leaf area index, LAI; percent  
607 groundcover, %GC; and species). Note that the AP site only had four plots with the data required  
608 for the analysis.

Site	Plot	LAI	%GC	Species	$\beta_s$ (cm)	$R_2$ ( $\Delta\theta$ - $P$ )	$P$ (cm)	$I_a/P$
AP	2	1.65	47.6	SF Slash	0.620	0.31	145.0	0.206
AP	3	0.90	62.8	SF Slash	0.014	0.78	145.0	0.06
AP	4	1.35	49.1	SF Slash	0.445	0.67	145.0	0.184
AP	6	0.40	73.4	Longleaf	0.014	0.57	145.0	0.06
DH	1	0.85	86.2	Loblolly	0.170	0.90	131.5	0.121
DH	2	2.48	51.2	Slash	0.621	0.68	131.5	0.211
DH	3	1.40	39.2	Slash	0.249	0.49	131.5	0.144
DH	4	3.31	35.8	Slash	0.464	0.71	131.5	0.188
DH	5	3.70	27.1	Loblolly	0.383	0.69	131.5	0.173
DH	6	3.48	32.9	Slash	0.418	0.40	131.5	0.18
EF	1	0.12	13.6	Clearcut	0.099	0.93	153.8	0.084
EF	2	1.05	56.9	Slash	0.092	0.96	153.8	0.081
EF	3	2.50	11.8	Sand	0.086	0.93	153.8	0.079
EF	4	0.66	50.9	Slash	0.094	0.92	153.8	0.082
EF	5	0.81	17.9	Sand	0.085	0.96	153.8	0.078
EF	6	0.52	52.0	Longleaf	0.076	0.89	153.8	0.075
GS	1	1.07	67.9	Clearcut	0.502	0.84	132.4	0.199
GS	2	2.66	7.9	Slash	0.535	0.88	132.4	0.203
GS	3	2.11	71.5	Slash	0.587	0.82	132.4	0.211
GS	4	1.12	42.4	Slash	0.421	0.90	132.4	0.185
GS	5	1.17	45.6	Slash	0.382	0.76	132.4	0.178
GS	6	0.51	55.2	Longleaf	0.339	0.78	132.4	0.169
LF	1	0.26	43.5	None	0.166	0.85	136.3	0.121
LF	2	2.86	23.1	Slash	0.525	0.64	136.3	0.195
LF	3	1.23	24.9	Slash	0.266	0.72	136.3	0.147
LF	4	0.80	25.7	Slash	0.248	0.64	136.3	0.143
LF	5	2.60	12.3	Slash	0.443	0.63	136.3	0.182
LF	6	0.89	25.9	Longleaf	0.458	0.69	136.3	0.184
LR	1	0.46	34.0	Clearcut	0.151	0.96	144.5	0.099
LR	2	2.97	38.1	Slash	0.429	0.84	144.5	0.162
LR	3	0.92	47.0	Slash	0.173	0.95	144.5	0.106
LR	4	2.52	26.7	Slash	0.232	0.92	144.5	0.122
LR	5	1.55	28.1	Slash	0.177	0.96	144.5	0.107
LR	6	1.16	35.5	Longleaf	0.160	0.96	144.5	0.102

609

610 Table 2. Summary of generalized linear model (GLM) results for interception storage capacity  
 611 ( $\beta$ s). LAI is leaf area index, GC is groundcover, and WT is water table (shallow vs. deep). The  
 612 best model (by AIC) is shown in bold.

Model #	Variable(s)	AIC	R <sub>2</sub>
1	LAI	378.1	0.32
2	LAI + site	318.5	0.66
3	LAI * site	255.9	0.83
<b>4</b>	<b>LAI * site + GC</b>	<b>253.1</b>	<b>0.84</b>
5	LAI + WT	338.3	0.55
6	LAI * WT	339.8	0.55
7	LAI * WT + GC	341.8	0.55
8	LAI + WT + GC	340.3	0.55

613